Chemical Engineering Journal 210 (2012) 547–556

Contents lists available at SciVerse ScienceDirect

Chemical Engineering Journal

journal homepage: www.elsevier.com/locate/cej

# Activated coke impregnated with cerium chloride used for elemental mercury removal from simulated flue gas

Shasha Tao, Caiting Li *, Xiaopeng Fan, Guangming Zeng, Pei Lu, Xing Zhang, Qingbo Wen, Weiwei Zhao, Diqiang Luo, Chunzhen Fan

*College of Environmental Science and Engineering, Hunan University, Changsha 410082, PR China*
*Key Laboratory of Environmental Biology and Pollution Control, Hunan University, Ministry of Education, Changsha 410082, PR China*

## HIGHLIGHTS

- AICC was developed for effective $Hg^0$ removal from simulated flue gas.
- The AICC samples possessed a joint oxidation effect on $Hg^0$ removal.
- The Hg species adsorbed on AICC samples were identified mainly as HgO and $HgCl_2$.
- The roles of $O_2$, NO, $SO_2$ and $H_2O$ (g) in $Hg^0$ oxidation by AICC were explored.

## ARTICLE INFO

*Article history:*
Received 31 May 2012
Received in revised form 27 August 2012
Accepted 10 September 2012
Available online 20 September 2012

*Keywords:*
Elemental mercury
Activated coke
Catalytic oxidation
Cerium chloride

## ABSTRACT

Gas-phase elemental mercury ($Hg^0$) removal by activated coke impregnated with cerium chloride (AICC) was studied under simulated flue gas conditions. Brunauer–Emmett–Teller (BET), X-ray diffractogram (XRD), scanning electron microscopy with energy dispersive X-ray spectrometry (SEM-EDX) and X-ray photoelectron spectroscopy (XPS) analyses were used to characterize the samples. The effects of $CeCl_3$ loading values, reaction temperatures and individual flue gas components including $O_2$, NO, $SO_2$ and $H_2O$ (g) on $Hg^0$ removal efficiency of AICC samples were investigated. Results showed that $Hg^0$ removal efficiency of AC was significantly enhanced by $CeCl_3$. The optimal $CeCl_3$ loading value and reaction temperature was around 6% and 170 °C, respectively. Additionally, the experiment results of effects of flue gas components on $Hg^0$ removal efficiencies showed that when $O_2$ was present in the flue gas, NO and $SO_2$ were observed to promote $Hg^0$ oxidation. However, in the absence of $O_2$, $SO_2$ showed an insignificant inhibition on $Hg^0$ removal. Furthermore, when $H_2O$ was added into the flue gas, the $Hg^0$ removal capacity had a slight declination. The analyses of XRD and XPS showed that $Ce_xO_y$ and C–Cl were generated on the surface of AICC and those active elements had remarkably positive effects on the $Hg^0$ removal. The reaction mechanism indicated that $Hg^0$ oxidation was achieved through two pathways: one was that $Hg^0$ bond with $CeO_2$ and was converted by the catalytic oxidation of valence variable cerium; the other was that $Hg^0$ reacted with C–Cl on the sample and was oxidized favored by chloride presence. And according to Hg 4f XPS analysis, the mercury on the surface of AICC was mainly in the form of mercuric oxide (HgO) and mercuric chloride ($HgCl_2$).



## 1. Introduction

Mercury emitted from coal-fired utility boilers has become a significant environmental issue because of its volatility, persistence, bioaccumulation and high toxicity [1–3]. On April 19, 2012, the US Environment Protection Agency (EPA) issued the national standard *Final Mercury and Air Toxics Standards* for the control of mercury, acid gases, and other toxic pollution from coal-fired power plants [4]. In addition, the State Environmental Protection Administration of China (SEPA) also initiated the *Emission Standard of Air Pollution for Thermal Power Plants* (GB13223-2011), in which the limit of mercury emission from coal-fired power plants is 0.03 $mg/m^3$ [5]. Therefore, it is required to develop effective technologies to govern mercury emission from coal-fired utility [6].

Mercury removal in coal-fired utilities greatly depends on its speciation in the post-combustion flue gases [7]. Mercury in coal-fired flue gas is often present as elemental mercury ($Hg^0$), oxidized mercury ($Hg^{2+}$), and particle-bound mercury ($Hg^P$). Thereinto, $Hg^P$

* Corresponding author at: College of Environmental Science and Engineering, Hunan University, Changsha 410082, PR China. Tel./fax: +86 731 88649216.
*E-mail addresses:* ctli@hnu.edu.cn, ctli3@yahoo.com (C. Li).

1385-8947/$ - see front matter © 2012 Elsevier B.V. All rights reserved.
http://dx.doi.org/10.1016/j.cej.2012.09.028

and $Hg^{2+}$ are relatively easy to be captured by the existing air pollution control devices (APCDs). For example, along with fly ash particles, $Hg^P$ can be captured by the particulate matter (PM) control devices such as electrostatic precipitators (ESPs), and fabric filters (FFs). $Hg^{2+}$ is water-soluble and thus can be removed by the wet flue gas desulfurization devices (WFGDs) with high efficiency. However, $Hg^0$ is much difficult to be captured by APCDs because of its high volatility and nearly insolubility in water. Thus, comparing with the capture of other forms of mercury, the capture of $Hg^0$ is the most practical challenge [8–11].

Up to present, numerous technologies have been researched to capture $Hg^0$ from the flue gas [12]. Thereinto, activated carbon injection (ACI) is widely applicable for $Hg^0$ emission control, particularly using activated carbons treated by sulfur, chloride or iodine [13–15]. In addition, metal oxides, such as CuO, $Cr_3O_4$, $MnO_2$, $Fe_2O_3$, $TiO_2$ and $V_2O_5$, modified activated carbons have also been extensively investigated and showed a promising performance in heterogeneous oxidation of $Hg^0$ [16–21]. However, the application and development of ACI is limited due to its higher price and lower utilization rate. Moreover, the mixing of the discharged activated carbon with fly ash increases the carbon content and affects the utilization of fly ash as a concrete extender, or even worse, it may result in environmental problems due to $Hg^0$ release from concrete afterwards [22,23].

It has been reported that activated coke (AC) is effective for simultaneous removal of $SO_2$, $NO_x$ and $Hg^0$ from flue gas at temperatures of 100–200 °C [24,25]. With high mechanical strength, AC could resist abrasion and crushing during the circulation and handling process [24,25]. Compared to the conventional activated carbon, the price of AC was lower and the used AC could be regenerated [24,26,27]. In addition, the catalytic properties of both fresh and used AC (after $SO_2$ treatment) are superior to those of conventional activated carbons [24,25,27]. In our previous works, $CeO_2$ was found to have superior activity and stability on $Hg^0$ capture because of its large oxygen storage capacity and unique redox couple $Ce^{3+}/Ce^{4+}$ [28–30]. $CeO_2$ can act as an oxygen reservoir by storing or releasing O via the $Ce^{4+}/Ce^{3+}$ redox couple, and thence it has become a very important catalyst in $Hg^0$ removal reaction [31]. Furthermore, it has been found that HCl is a most important species affecting mercury oxidation [3] since the major oxidized mercury in coal-derived flue gas is $HgCl_2$. However, the concentration of HCl in the flue gas derived from subbituminous or lignite coal-burning units is low [32]. According to the previous studies [15,33,34], the impregnated Cl element was strongly supportive for activated carbon to adsorb $Hg^0$. Therefore, the use of chloride as an active element may be an effective option to enhance mercury removal efficiency. In this study, cerium chloride ($CeCl_3$), as the precursor of $CeO_2$ and supporter of Cl, was loaded on activated coke and the $Hg^0$ retention and oxidation ability of the $CeCl_3$-impregnated samples were investigated and evaluated in fixed-bed system to produce effective mercury adsorbent for coal-fired utilities.

## 2. Experimental section

### 2.1. Samples preparation

The AC was obtained from Inner Mongolia KeXing Carbon Industry Limited Liability Company. The $CeCl_3$-impregnated samples were prepared by the equivalent-volume impregnation of AC with $CeCl_3$ aqueous solution as follows: At first, the AC was ground and sieved into 100–120 mesh size. Then, the powdered virgin AC was washed with de-ionized (DI) water and dried in an electric blast oven at 105 °C for 12 h. After that, different amount of $CeCl_3{\cdot}7H_2O$, according to $CeCl_3$ loading value ($\rho$) varied from 2% to 10%, was dissolved in de-ionized water and the AC was impregnated in the solution for 24 h. After impregnation, the samples were dried in an electric blast drying oven at 120 °C for 24 h. Finally, the samples were cooled down to ambient temperature and stored in a desiccator. The $CeCl_3$-impregnated samples were denoted as AICC*x*, where A represents Activated coke, I represents Impregnation, CC represents $CeCl_3$ and *x* represents the weight percentage of the $CeCl_3$, respectively.

### 2.2. Samples characterization

Brunauer–Emmett–Teller (BET) specific surface area of the samples was determined by nitrogen adsorption at −196 °C on a Micromeritics ASAP 2010 analyzer. The average pore diameter and pore volume were obtained from nitrogen adsorption isotherm. All of the samples were degassed at 120 °C prior to BET measurements.

X-ray diffractogram (XRD) measurements were carried out on Siemens D5000 powder diffractometer to examine the crystallinity and dispersivity of cerium species on the support. The XRD patterns were obtained in the $2\theta$ range from 10 to 80 with $2°min^{-1}$ scanning rate and 0.02° data interval, using nickel-filtered Cu K$\alpha$ ($\lambda$ = 1.54 Å) radiation as an X-ray source. The accelerating voltage and the applied current were 35 kV and 30 mA, respectively.

To further analyze the morphology and surface structure of the samples, scanning electron microscopy (SEM) photographs were obtained by means of FEI-Sirion200 after vacuum plating Au film. With the attachment of energy dispersive X-ray spectrometry (EDX), the semi-quantitative elemental analysis of samples can be supported with high resolution. Three separated areas for each sample were magnified to 5000X, and an image was obtained (only one area was analyzed for the selected samples).

X-ray photoelectron spectroscopy (XPS) analysis was performed at room temperature on a VGMultilab 2000 spectrometer (Thermo Electron Corporation, USA) with an Mg K$\alpha$ X-ray source. The binding energies were calibrated by the C 1s peak at 284.6 eV.

### 2.3. Experimental setup and procedure

Fig. 1 shows the experimental setup for evaluating $Hg^0$ removal on the AICC samples. The test rig was composed of a simulated flue gas feed system, an $Hg^0$ vapor-generating device, a fix-bed furnace device and an online mercury analyzer. The standard composition of the basic flue gas including 25.73 $\mu g/m^3$ $Hg^0$, 4% $O_2$, 8% $H_2O$, 12% $CO_2$, 300 ppm NO, 400 ppm $SO_2$ and balanced $N_2$. The total flow rate was controlled at 1 L/min in each experiment using a mass flow controller and the space velocity (SV) was around $2.4 \times 10^4\ h^{-1}$. The peristaltic pump transferred water into the stainless steel tube wrapped with a heating line and then $H_2O$ (g) was generated. The $Hg^0$ vapor-generating device consisted of an elemental mercury permeation tube (VICI Metronics) and a water bath. The $Hg^0$ permeation tube was placed in a U-shaped glass tube, which was immersed in a water bath with a tunable temperature, and the tube was set to release steady $Hg^0$ vapor. The $N_2$ flow was divided into two branches: one branch converged with the $O_2$, $CO_2$, NO and $SO_2$ to form the main gas flow, while the other (300 mL/min) passed through the $Hg^0$ permeation tube and introduced the saturated $Hg^0$ vapor into the system.

The fixed-bed reactor was comprised of a digital temperature controller and a quartz tube with an inner diameter of 20 mm and a length of 60 cm. The digital temperature controller was employed to keep the fixed-bed reactor at the desired temperature. In each test, about 0.2 g sample was premixed with 1 g of silica (Fine granules, 40–100 mesh) and packed in the quartz tube. The exhaust gas from the mercury analyzer was introduced into the activated carbon trap before being expelled into the atmosphere.

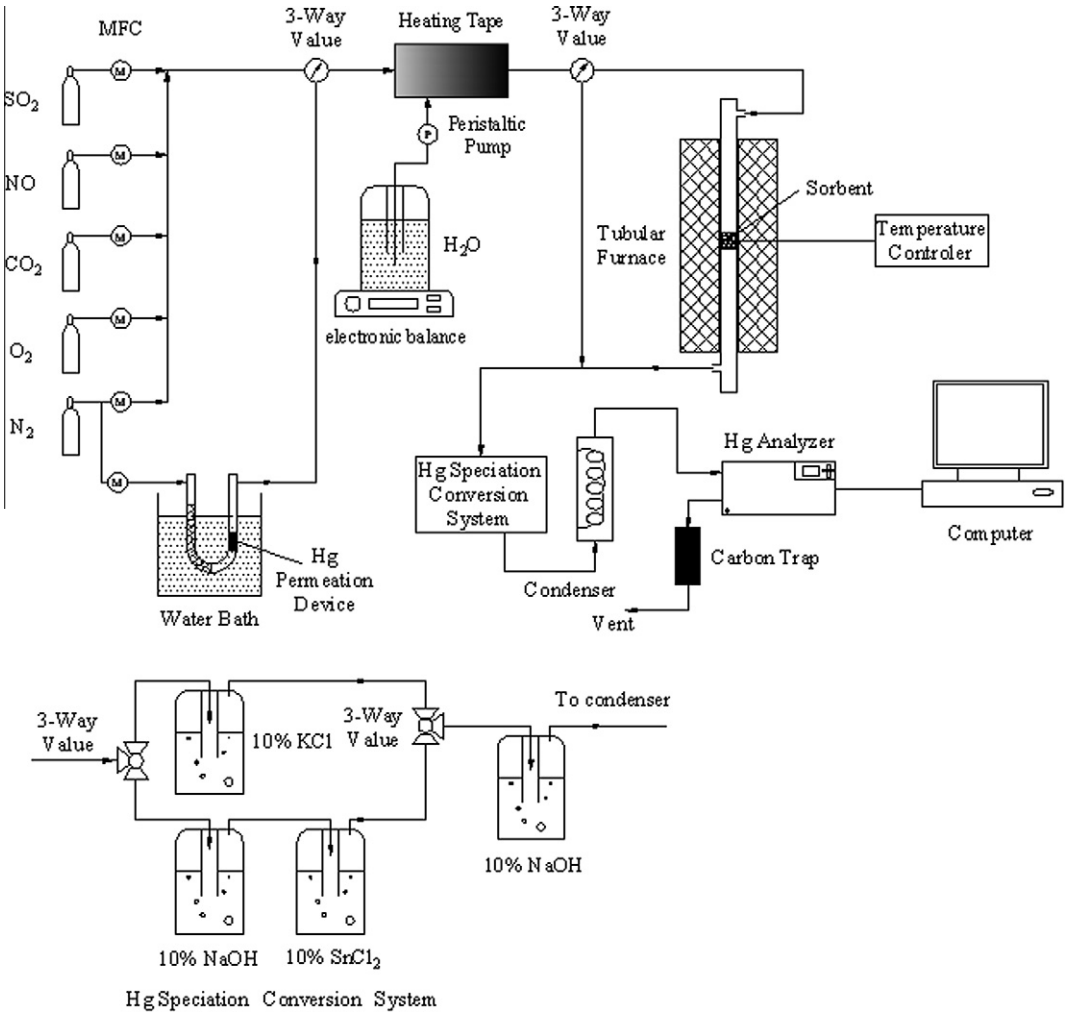


**Fig. 1.** Schematic diagram of the experimental setup.

**Table 1**
Experimental conditions.

| | Sample | Carrier gas (1 L/min) | Temperature (°C) |
|---|---|---|---|
| Set 1 | AC, AICC2, AICC4, AICC6, AICC8, AICC10 | Simulated flue gas (SFG: 4% $O_2$, 8% $H_2O$, 12% $CO_2$, 300 ppm NO, 400 ppm $SO_2$) | 140 |
| Set 2 | The optimal sample | Simulated flue gas (SFG: 4% $O_2$, 8% $H_2O$, 12% $CO_2$, 300 ppm NO, 400 ppm $SO_2$) | 110–230 |
| Set 3 | The optimal sample | $N_2/(N_2 + O_2)$ + individual flue gas components (NO, $SO_2$); SFG (dry); SFG (8% $H_2O$) | The optimal reaction temperature |

A blank test was carried out in order to examine the adsorption of $Hg^0$ on the tubing, reactor, and the blank silica prior to the main experimental study on mercury uptake by samples. Results showed that the $Hg^0$ adsorption efficiency of the blank was below 1% over the range of temperatures from 110 to 230 °C.

Three sets of experiments were conducted and the conditions are listed in Table 1. Set 1 experiments aimed at determining the optimal $CeCl_3$ loading value on AC. The $Hg^0$ removal activities over virgin AC and AICC samples were evaluated under simulated flue gas (SFG: 4% $O_2$, 8% $H_2O$, 12% $CO_2$, 300 ppm NO, 400 ppm $SO_2$, and 25.73 μg/$m^3$ $Hg^0$) for 3 h. In Set 2, the optimal sample was tested in SFG at each selected reaction temperatures from 110 to 230 °C for investigating the optimal reaction temperature. The roles of individual flue gas components in $Hg^0$ removal and the reaction pathways were explored in Set 3 experiments, which were conducted on the optimal sample in the presence of individual flue gases (balanced with $N_2$ or $O_2$ plus $N_2$) at optimal operating temperature. Please note that HCl gas was not added to the simulated flue gas for all the Sets of experiments listed in order to eliminate the well-known heterogeneous mercury oxidation [35].

During the experiments, $Hg^0$ concentration was online monitored by a RA-915 M Mercury Analyzer (LUMEX Ltd., Russia) which can measure solely the concentration of $Hg^0$. In order to measure the concentration of the total mercury ($Hg^T$) including both elemental and oxidized mercury in reactant gases, a mercury specification conversion system was coupled to the RA-915 M Mercury Analyzer. According to the procedure reported by Li et al. [36], in the mercury specification conversion system, the sampling gas was divided into two streams. On the one stream, an impinger with 10 wt% potassium chloride (KCl) solution, which captured $Hg^{2+}$ and allowed only $Hg^0$ to pass through, was used for $Hg^0$ measurement. On the other stream, an impinger containing 10 wt% stannous

chloride ($SnCl_2$) solution, whose pH was about 0.5, was located to measure $Hg^T$. After passing the solution, all oxidized mercury species were reduced to $Hg^0$ via the acidic $SnCl_2$ solution and the concentration of the total mercury could be measured. In order to remove $SO_2$, which could interfere with the reduction of $Hg^{2+}$ by $SnCl_2$, a 10 wt% sodium hydroxide (NaOH) solution was used before the sampling gas entered the $SnCl_2$ solution. The concentration of $Hg^{2+}$ could then be calculated by the difference between $Hg^T$ and $Hg^0$. Interferences on the $Hg^0$ measurement by the empty reactor and flue gas components were verified to be negligible. Even so, at the end of the conversion system, the sample flow sequentially entered a 10 wt% NaOH solution in which acid gases were captured and a condenser by which $H_2O$ could be removed to avoid corrosion of the detection cell in the mercury analyzer.

Our hypothesis was that the surface deposit of mercury was thoroughly in the oxidized state. Therefore, the $Hg^0$ oxidation efficiency ($E_{oxi}$) is calculated by the following formula:

$$E_{oxi}(\%) = \frac{\Delta[Hg^0]}{[Hg^0]_{in}} = \frac{[Hg^0]_{in} - [Hg^0]_{out}}{[Hg^0]_{in}} \times 100\% \quad (1)$$

where $[Hg^0]_{in}$ and $[Hg^0]_{out}$ represent $Hg^0$ concentration at the inlet and outlet of the reactor, respectively. All or part of the $\Delta Hg^0$ is captured on the samples as solid phase and the rest escapes to the gas phase. Thus, the $Hg^0$ capture efficiency ($E_{cap}$) is always less than or equal to $E_{oxi}$, with $E_{cap}$ defined as

$$E_{cap}(\%) = \frac{\Delta[Hg^T]}{[Hg^T]_{in}} = \frac{[Hg^T]_{in} - [Hg^T]_{out}}{[Hg^T]_{in}} \times 100\%$$

$$\text{or } E_{cap}(\%) = \frac{[Hg^0]_{in} - [Hg^T]_{out}}{[Hg^0]_{in}} \times 100\% \quad (2)$$

where $[Hg^T]_{in}$ and $[Hg^T]_{out}$ represent $Hg^T$ concentration at inlet and outlet of the reactor, respectively. Note that in this study $[Hg^T]_{in} = [Hg^0]_{in}$ and $[Hg^T]_{out} \geqslant [Hg^0]_{out}$.

The experimental error is inevitable. Hence, $E_{oxi}$ and $E_{cap}$ are the average of three or more replicates and the error bars in the figures represent the standard deviation from the mean of the series of experiments at each condition.

## 3. Results and discussion

### 3.1. Samples characteristics

The physical properties of virgin AC and AICC including BET surface area, total pore volume and average pore size are summarized in Table 2. It could be seen that the virgin AC showed the highest BET surface area ($S_{BET}$) of 395.79 $m^2/g$ and the biggest total pore volume of 0.154 $cm^3/g$. However, the doping of $CeCl_3$ (2–10%) reduced the $S_{BET}$ and pore volume of AC to some extent. Especially, when the virgin AC was doped with 10 wt% $CeCl_3$, the $S_{BET}$ and the total pore volume value was reduced to 261.39 $m^2/g$ and 0.102 $cm^3/g$, respectively. The result could be explained as follows: with the increase of the $CeCl_3$ loading, $CeCl_3$ or other cerium compounds, which existed over the external surface of the samples, would deteriorate the thin pore walls and block internal pores [30]. But there was no apparent trend between the average pore size and the $CeCl_3$ loading.

**Table 2**
BET surface and pore parameters of the samples.

| Sample | Surface area ($m^2/g$) | Pore volume ($cm^3/g$) | Average pore size (nm) |
|---|---|---|---|
| AC | 395.79 | 0.154 | 19.884 |
| AICC2 | 377.78 | 0.147 | 19.764 |
| AICC4 | 351.15 | 0.136 | 19.895 |
| AICC6 | 334.19 | 0.129 | 19.827 |
| AICC8 | 296.73 | 0.114 | 20.128 |
| AICC10 | 261.39 | 0.102 | 19.748 |

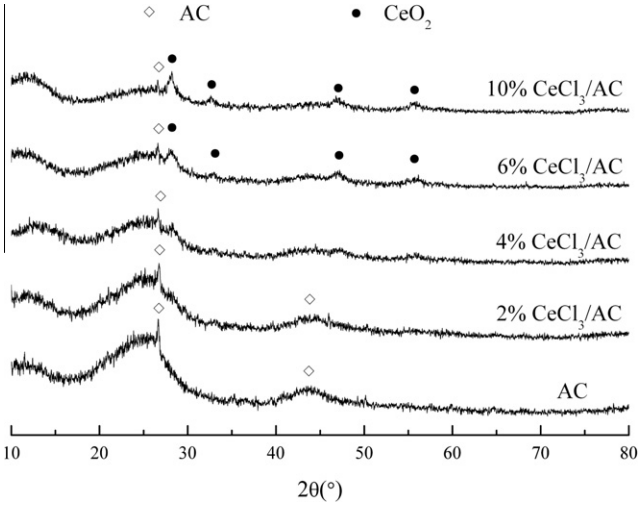


**Fig. 2.** XRD spectra of virgin AC and the AICC samples.

To identify the structure of cerium species on the samples, XRD measurements of virgin AC and AICC were conducted and the XRD patterns are shown in Fig. 2. For virgin AC, two strong diffraction peaks were detected at $2\theta = 26.66°$ and 44.58°. However, the intensity of the two peaks decreased with the increase of $CeCl_3$ loadings and the peak at $2\theta = 44.58°$ was even disappeared when the loading above 4%. This could indicate that $CeCl_3$ and AC had strong interaction in these samples. The peaks at the ranges of $2\theta = 27.88°$, 32.96°, 46.98° and 56.14° in the XRD patterns were corresponding to the specific peaks of $CeO_2$, which could be detected over AICC6 and AICC10. But no apparent peak due to $CeCl_3$ was observed over all of the AICC samples. This could indicate that $CeCl_3$, as a precursor, was extensively converted to $CeO_2$ in the preparation of AICC. Moreover, there were no apparent characteristic peaks ascribable to $CeO_2$ over AICC2 and AICC4. According to the monolayer dispersion theory [37], when the oxide content was in the range of the threshold value, the oxide was in a monolayer dispersion state and, when the content of oxide was more than the threshold value, the oxide was in a crystalline phase. Hence, it was concluded that $CeO_2$ was highly dispersed on the surface of AC when the loading value was less than 6%. Furthermore, a weak crystal phase of $CeO_2$ was detected for AICC6 and the intensity of the peaks increased with the growth of cerium loading, powerfully indicating that the surface of AC was occupied by $CeO_2$ as the $CeCl_3$ loading increased to somewhere between 4% and 6%.

Fig. 3 shows the SEM micrographs of virgin AC and the selected AICC samples. The characteristics of the AC surface have changed according to chemical loading. The dark zones indicated carbon enriched areas, while light zones demonstrated the presence of metal oxides. As shown in Fig. 3, cerium oxide was highly dispersed on the AC surface and only a few cerium oxide agglomerates existed in AICC6. Especially, for AICC10, the white agglomerates were more apparent. The results were in accordance with the XRD results. Furthermore, there were more small holes in the surface of the AICC samples, which indicated that cerium chloride extensively modified the structure of AC. The results of the SEM-EDX analysis, presented in Table 3, shows that the content of Cl plus Ce was a little higher than the calculated content, which may be because that the SEM-EDX just determined the surface layer morphology and composition of the samples. Moreover, it could be found that the molar

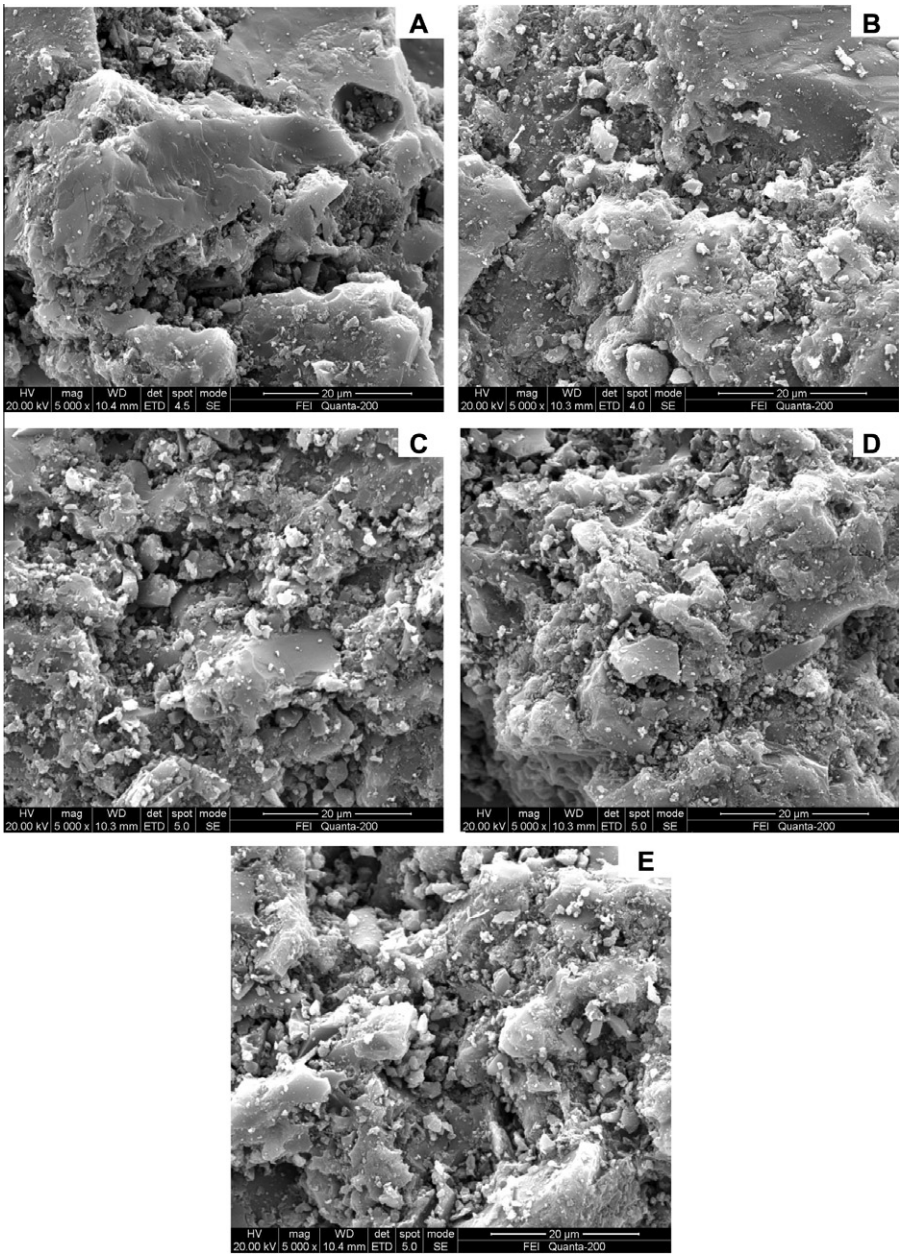


**Fig. 3.** SEM micrographs of (A) virgin AC, (B) AICC2, (C) AICC4, (D) AICC6 and (E) AICC10.

**Table 3**
Surface atomic content of virgin AC and the AICC samples.

| Sample | Surface atomic content (wt%) | | | | | |
|---|---|---|---|---|---|---|
| | C | O | Al | Si | Cl | Ce |
| AC | 86.36 | 7.49 | 2.57 | 3.58 | 0.00 | 0.00 |
| AICC2 | 85.20 | 7.60 | 1.96 | 2.62 | 0.79 | 1.83 |
| AICC4 | 84.43 | 6.35 | 1.61 | 2.23 | 1.89 | 3.49 |
| AICC6 | 83.22 | 6.34 | 1.25 | 1.77 | 1.84 | 5.58 |
| AICC10 | 81.10 | 4.61 | 0.89 | 1.43 | 3.43 | 8.54 |

ratio of Cl and Ce ($n_{Cl}$:$n_{Ce}$) was lower than 3:1. The loss of Cl atoms would be due to the following two reasons: one was that Cl, in the form of HCl, was released during the preparation of the samples and the other was that Cl atoms were bond to inside layer of the support and therefore, could not be detected.

Fig. 4 shows the XPS spectra of Hg 4f, Cl 2p, Ce 3d and O 1s on the samples with and without adsorbed mercury. The spectrum of Hg captured on AICC6 under the condition of set 2 at the temperature of 170 °C showed two peaks at around 104.4 and 101.4 eV. A strong peak at 102.9 eV was ascribed to the Si 2p electron. The mercury and silicon profiles were obtained by separating the overlapped Hg 4f and Si 2p ($SiO_2$) signals using peak fitting (Fig. 4a). The Hg $4f_{7/2}$ binding energy identified as 101.4 ± 0.2 eV was significantly higher than the 99.9 eV reference point for $Hg^0$ [38]. This inferred that there must be no $Hg^0$ on the $CeCl_3$-impregnated AC samples and the result was generated from the heterogeneous oxidation of $Hg^0$, changing from the $Hg^0$ in the gas phase to $Hg^{2+}$ in the adsorbed phase. The higher binding energies for Hg $4f_{5/2}$ and Hg $4f_{7/2}$ on the samples can be attributed to HgO (with the peak at 104.4 eV) and $HgCl_2$ (101.4 eV) [38,39]. Thus, it was concluded that the $Hg^0$ oxidation of AICC could be mainly influenced by the O and Cl species on the samples surface.

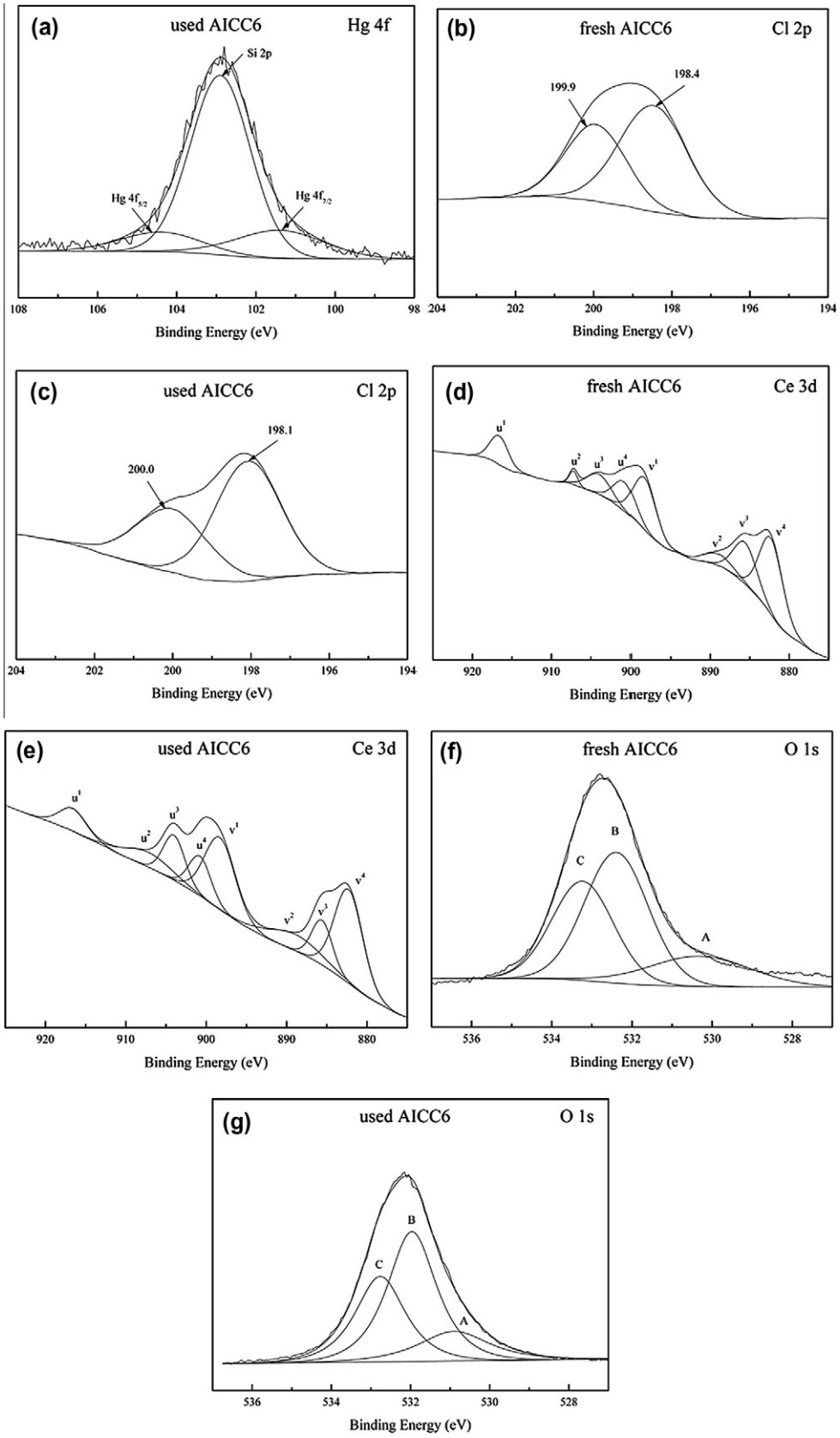


**Fig. 4.** Hg 4f, Cl 2p, Ce 3d and O 1s XPS spectra of fresh AICC6 and used AICC6 (The sample was subjected to $Hg^0$ removal under the condition of Set 2 with the temperature of 170 °C).

As showed in Fig. 4b, two main peaks centered at about 199.9 and 198.4 eV were assigned to C–Cl moieties and ionic $Cl^-$ moieties, respectively [40–42]. The appearance of C–Cl moieties illustrated that a portion of Cl in the $CeCl_3$ was reduced by the carbon content in AC and presented as C–Cl moieties. The ratio of the spectra area with respect to C–Cl and $Cl^-$ was about 0.65 for the blank sample without mercury, but the ratio decreased to 0.57 for the used sample. This indicated that some of the C–Cl was converted to $Cl^-$ by reacting with $Hg^0$ during the adsorption process and possibly existed as $HgCl_2$ which presents in the Hg XPS spectra.

The XPS spectra of Ce 3d for AICC6 with and without adsorbed mercury were presented in Fig. 4e and d. XPS peaks denoted as u are due to $3d_{3/2}$ spin-orbit states and those denoted as v are the corresponding $3d_{5/2}$ states. The u/v, $u^2/v^2$, and $u^3/v^3$ doublets are attributed to $3d^{10}4f^0$ state of $Ce^{4+}$, while the doublet labeled $u^1/v^1$ represents the $3d^{10}4f^1$ initial electronic state corresponding to $Ce^{3+}$ [36]. In the fresh sample, peaks attributed to $Ce^{3+}$ and $Ce^{4+}$ were observed, which was well consistent with the XRD results. The appearance of $CeO_2$ and $Ce_2O_3$ made the unique redox couple $Ce^{3+}/Ce^{4+}$ composed and within the redox shift between $Ce^{3+}$ and $Ce^{4+}$, labile oxygen vacancies and bulk oxygen species with relatively high mobility could be easily generated [43], which were active for oxidation process. The ratio of the spectra area of $Ce^{3+}$–$Ce^{4+}$ was 0.32, indicating that the $Ce^{4+}$ oxide was the main form in the fresh sample. In comparison with the fresh sample, the ratio of $Ce^{3+}$–$Ce^{4+}$ decreased to 0.24 for the sample with adsorbed mercury, implying that the conversion from $Ce^{3+}$ to $Ce^{4+}$ was predominant within the redox shift between $Ce^{3+}$ and $Ce^{4+}$.

The XPS spectra of O 1s on the samples are showed in Fig. 4f and g. There are three overlapping peaks observed. The weak peak of O 1s A, with a binding energy of about 530.0 eV, ascribes to the lattice oxygen ($O^{2-}$) in the metal oxide. The strong peak at around 531.7 eV represents the chemisorbed oxygen or/and weakly bonded oxygen species (O 1s B), which are the most active oxygen and play an important role in oxidation reaction [36]. Field investigations have shown that $Ce^{3+}$ could create a charge imbalance, vacancies and unsaturated chemical bonds on the sample surface, for which more chemisorbed oxygen or/and weakly bonded oxygen species would be brought [31,36]. The peak with a binding energy of about 532.6 eV belongs to surface oxygen in hydroxyl species and/or adsorbed water species presser as contaminants at the surface (O 1s C) [44]. According to previous works, many hydroxyl groups were present in the surface of AC [25]. It can be observed that $O_B/O_T$ ($O_T$ denoted the atomic concentration of total oxygen) increased from 0.46 to 0.51 after the adsorption and oxidation reaction. Considering the peak of HgO at 104.4 eV, it was proposed that the weakly adsorbed mercury might be bonded with these weakly adsorbed O-oxygen species.

### 3.2. Performance of the catalyst-loaded sorbent

#### 3.2.1. Effect of loading value

Fig. 5 presents the effects of $CeCl_3$ loading value on $Hg^0$ removal efficiencies of AICC. It was clear that $CeCl_3$ significantly enhanced the $Hg^0$ removal ability of AC and the averaged $E_{oxi}$ and $E_{cap}$ improved with the increase of $CeCl_3$. Table 2 shows that the $S_{BET}$ and pore volume reduced with the increase of $CeCl_3$ loading and the optimal samples (AICC6) showed a relatively low $S_{BET}$ and pore volume. It indicated that the $Hg^0$ removal of AICC was mainly influenced by the oxidation of AICC and less affected by the $S_{BET}$ of AICC, which could affect the physisorption of AICC for mercury. And this was in line with the results of Fig. 4. Moreover, in the preparation of AICC, $CeCl_3$ could bring a large amount of $CeO_2$ and C–Cl functional groups. So it was concluded that the oxidation capacity of AICC was mainly dependent upon the $CeO_2$ and C–Cl on the surface

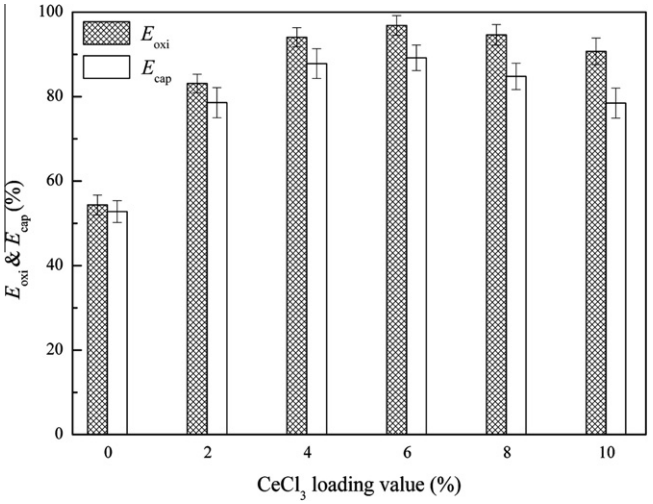


**Fig. 5.** Effect of $CeCl_3$ loading value on $Hg^0$ removal efficiency.

of the sample. This was similar to other investigations [15,29,45], which showed that $CeO_2$ and C–Cl were more important for the oxidation of $Hg^0$. Additionally, when the $CeCl_3$ loading value exceeds 6%, the averaged $E_{oxi}$ and $E_{cap}$ decreased. It could be found from Fig. 2 that when the $CeCl_3$ loading was above 6%, there were more aggregation of excessive cerium compounds which made the $S_{BET}$ and pore volume dropped roughly, thus leading to the decrease of $E_{oxi}$ and $E_{cap}$. This indicated that the physisorption of AICC played some roles in $Hg^0$ removal. From the above, it was concluded that the $Hg^0$ removal was attributed to the combined action of physisorption and oxidation of AICC. Specially, the reaction mechanism of $Hg^0$ removal by AICC could be explicated as follows: During the impregnation of AC with $CeCl_3$ aqueous solution, $Cl^-$ was chemisorbed with carbon content in the activated coke and a few C–Cl functional groups were formed. Meanwhile, $CeO_2$ was generated by hydrolysis of $CeCl_3$, in which $CeO_2$ and HCl were generated as $CeCl_3$ reacted with water and oxygen in the air while being heated up. The reactions could be expressed as follows:

$$Cl^- + C \rightarrow C{-}Cl \quad (3)$$

$$4CeCl_3 + 6H_2O + O_2 \rightarrow 4CeO_2 + 12HCl \quad (4)$$

During the reaction, the gaseous $Hg^0$ was firstly adsorbed on the samples by the physisorption of AICC to form $Hg^0(ad)$; then $Hg^0(ad)$ would be further converted through two pathways: one was that $Hg^0(ad)$ reacted with C–Cl on the sample to form HgCl, which was further oxidized to $HgCl_2$ by another active species [15,45]; and the other was that $Hg^0(ad)$ would bind with the $CeO_2$ to form HgO [29]. The consumption of the $CeO_2$ by $Hg^0$ over the samples could be compensated by activating the gaseous oxygen from the flue gas. The series reaction for chemisorption of $Hg^0$ could be speculated as follows:

$$Hg^0 + AC - surface \rightarrow Hg^0(ad) \quad (5)$$

$$Hg^0(ad) + C{-}Cl \rightarrow HgCl + C \quad (6)$$

$$HgCl + C{-}Cl \rightarrow HgCl_2 + C \quad (7)$$

$$Hg^0(ad) + 2CeO_2 \rightarrow HgO + Ce_2O_3 \quad (8)$$

$$Ce_2O_3 + 1/2O_2 \rightarrow CeO_2 \quad (9)$$

The reactions indicated that activated coke loaded with cerium chloride possessed a joint effect on $Hg^0$ oxidation. One was the catalytic oxidation of valence variable cerium and the other was $Hg^0$ oxidation favored by chloride presence. From the Hg XPS analysis, the ratio of the spectra area with respect to HgO and $HgCl_2$ was

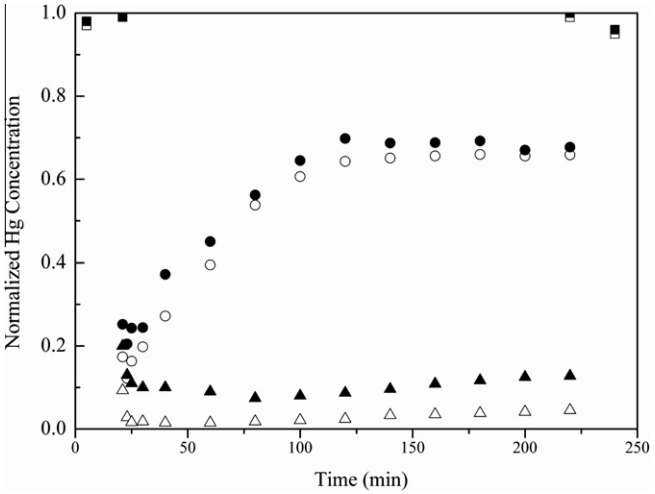


**Fig. 6.** Effect of reaction time on $Hg^0$ removal efficiencies of virgin AC and AICC6. Legend: ■, $[Hg^T]_{in}$; □, $[Hg^0]_{in}$; ●, $[Hg^T]_{out}$ – virgin AC; ○, $[Hg^0]_{out}$ – virgin AC; ▲, $[Hg^T]_{out}$ – AICC6; △, $[Hg^0]_{out}$ – AICC6.

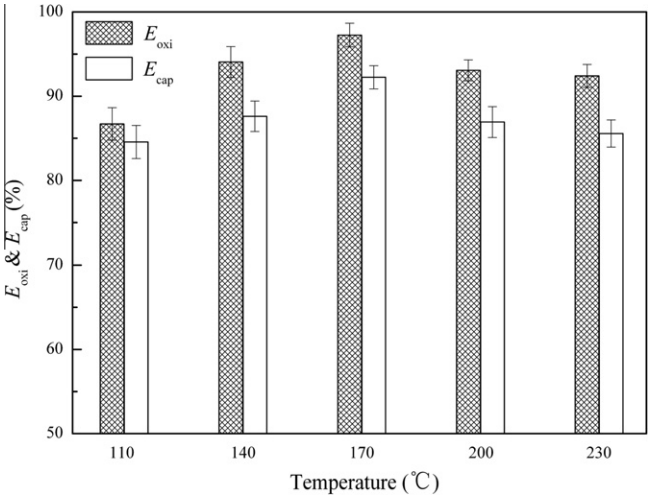


**Fig. 7.** Effect of reaction temperature on $Hg^0$ removal of AICC6.

about 1:1.55. It could be concluded that the adsorbed mercury was mainly in the form of $HgCl_2$ on the sample surface, which accordingly implied that C–Cl may play a main role in the first period of the $Hg^0$ removal process. But as the reaction progress, C–Cl could be gradually consumed by $Hg^0$ oxidation. Hence, the main role would probably shift from C–Cl to $CeO_2$ after a period.

It should be noted that $E_{cap}$ was lower than $E_{oxi}$ for these samples, which may be resulted from that a fraction of certain volatile Hg compounds (such as mercuric nitrate, $Hg(NO_3)_2$) were produced [46,47].

The profiles of normalized $Hg^0$ concentration as a function of time for virgin AC and the optimal AICC6 are shown in Fig. 6. At the beginning of each test, it could be found that $[Hg^T]_{in}$ and $[Hg^0]_{in}$ were very close to each other. After a 3 h period, $[Hg^T]_{in}$ and $[Hg^0]_{in}$ were checked again. For virgin AC, $[Hg^T]_{out}$ initially dropped to a low level ($E_{cap}$ = 75%), and then it increased to around 68% of $[Hg^T]_{in}$ ($E_{cap}$ = 32%) after 3 h. $[Hg^0]_{out}$ was found to slightly lower than $[Hg^T]_{out}$, indicating that a small portion of the captured $Hg^{2+}$ penetrated the reactor. At the end of the 3 h test, $Hg^0$ oxidation efficiency was around 34%. For AICC6, $[Hg^0]_{out}$ remained almost constantly below 6% of $[Hg^0]_{in}$ ($E_{oxi}$ > 94%). $[Hg^T]_{out}$ initially dropped to 10% of $[Hg^T]_{in}$, but gradually increased and stabilized around 13% ($E_{cap}$ = 87%). As noted above, the removal of $Hg^0$ was due to physisorption and oxidation. For AC, physisorption played a leading role in $Hg^0$ removal. With the reaction progressing, the physisorption gradually reduced and approached equilibrium. The reaction process of AICC6 illustrated that impregnated $CeCl_3$ could largely improve activated coke's $Hg^0$ removal ability and the activity performed good stability in 3 h. Moreover, comparing the $Hg^0$ removal efficiency of AICC6 with that of $CeO_2$/Activated Carbon and $CeO_2$/Activated Carbon Fiber, which had been studied in our previous experiments [28,29], it could be found that at the same period the $Hg^0$ removal efficiency of AICC6 was higher and more stable.

### 3.2.2. Effect of reaction temperature

The effect of reaction temperature on $Hg^0$ removal of AICC6 was examined over a range of temperatures from 110 to 230 °C and the results are given in Fig. 7. It could be seen that when the temperature rose from 110 °C to 170 °C, the averaged $E_{oxi}$ and $E_{cap}$ increased from about 86% and 84% to 97% and 92%, respectively. This manifested again that the $Hg^0$ removal of AICC was mainly influenced by its oxidation because the oxidation could boost and become the crucial factor with the increase of reaction temperature due to the formation of more chemical bonds. However, when the temperature continuously increased to 230 °C, the averaged $E_{oxi}$ and $E_{cap}$ decreased to 92% and 85%, respectively. This could be due to the inhibition of physisorption for $Hg^0$, which could be weakened by higher temperature. And it proved again that the $Hg^0$ removal was attributed to the combined action of physisorption and oxidation of AICC. It could be found that the optimal operating temperature was around 170 °C and $E_{oxi}$ and $E_{cap}$ were constantly above 80% in this temperature range during the 3 h test. These results manifested that a wide range of low temperatures was beneficial to the reaction between $Hg^0$ and chlorine/oxygen functional groups. As previous literatures clarified that mercury reacting with chloride showed exothermic behavior [15,48], thus the $Hg^0$ removal capability of chlorine functional groups would decrease with the increase of temperature. Nevertheless, the cerium dioxide possessed an optimal catalysis temperature for $Hg^0$ oxidation [29]. Therefore, it presented above trend when the effects of chloride and cerium dioxide on $Hg^0$ removal combined.

### 3.3. Effect of individual flue gas components

To explore the roles of individual flue gas components in $Hg^0$ removal and the reaction pathways, experiments (Set 3) were

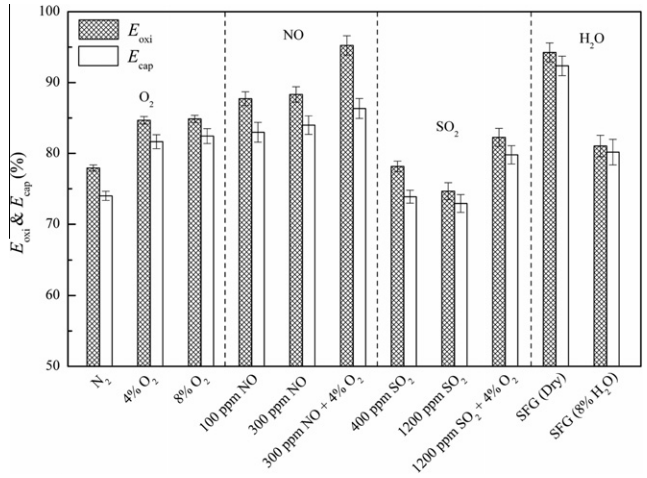


**Fig. 8.** Effects of individual flue gas components on $Hg^0$ oxidation and capture efficiency of AICC6 (all gases balanced with $N_2$).

conducted at the optimal temperature, 170 °C, by mixing $Hg^0$ with individual flue gas components and/or in combination with $O_2$, balanced with $N_2$. About 0.1 g of fresh AICC6 was used in each test. The results are summarized in Fig. 8.

*3.3.1. Effect of $O_2$*

$E_{oxi}$ and $E_{cap}$ over AICC6 under high purity $N_2$ (>99.999%) gas flow were observed to be around 78% and 74%, respectively, which were much higher than the $E_{oxi}$ and $E_{cap}$ observed over virgin AC in simulated flue gas. The loss of $Hg^0$ on the AICC6 in pure $N_2$ atmosphere was due to the reaction between $Hg^0$ and stored lattice Cl and O [49], which could act as oxidants to sustain oxidized mercury formation on the sample's surface even in the absence of $O_2$. When 4% $O_2$ was introduced to the gas flow, $E_{oxi}$ increased to 85%. But when $O_2$ concentration further increased to 8%, no obvious increase of $E_{oxi}$ was detected. This indicated that AICC6 sample could use the $O_2$ efficiently. Thus, low $O_2$ concentration would achieve the supplement of the lost lattice O and increasing the $O_2$ concentration made little difference.

*3.3.2. Effect of NO*

As illustrated in Fig. 8, 100 ppm NO resulted in 88% of $Hg^0$ oxidized and 83% captured. It has been revealed that $Ce^{3+}$ on the sample surface could promote the oxidation of NO–$NO_2$, and $NO_2$ was demonstrated to significantly improve heterogeneous oxidation of $Hg^0$ on fly ash and on activated carbon based sorbents [17,50]. However, increasing NO concentration to 300 ppm did not change $E_{oxi}$ and $E_{cap}$ substantially. It could be due to that oxygen stored on the AICC sample was limited for NO and $Hg^0$ oxidation. In addition, when 4% $O_2$ was added into the flue gas, the $E_{oxi}$ increased to 95%. Moreover, it should be noted that $E_{cap}$ was much lower than $E_{oxi}$. This indicated that besides $Hg^0$, a great amount of oxidized mercury could exist in the gas flow downstream of the AICC sample when flue gas contained NO. This was in agreement with previous proposal [36] that NO participated in the $Hg^0$ oxidation reaction and volatile mercuric compounds, like $Hg(NO_3)_2$, were generated. The pathway likely responsible for $Hg^0$ oxidation in the presence of NO is summarized below

$$NO + 1/2O_2 \rightarrow NO_2 \quad (10)$$

$$Hg^0 + NO_2 \rightarrow HgO + NO \quad (11)$$

$$Hg^0 + 2NO_2 + O_2 \rightarrow Hg(NO_3)_2 \quad (12)$$

Considering the much higher melting/decomposing point of $HgCl_2$ (277 °C) and HgO (500 °C), it was less likely for the penetration of these two less volatile Hg species. However, due to the low melting point of 79 °C, $Hg(NO_3)_2$ was likely to be volatile at the reactor temperature (170 °C) [46]. Accordingly, part of $Hg(NO_3)_2$ may be released from the reactor into the gas phase.

*3.3.3. Effect of $SO_2$*

The effect of $SO_2$ on $Hg^0$ oxidation/capture in the flue gas was complicated and not conclusive; either promotional or inhibitory effects have been reported in the literature [17,51,52]. Fig. 8 showed that when there was no $O_2$ in the flue gas, $SO_2$ slightly inhibited the $Hg^0$ conversion (about 1–4%). This could be due to the competition of $Hg^0$ and $SO_2$ for similar active sites on the sample surface. However, when 4% $O_2$ and 1200 ppm $SO_2$ were added into the simulated flue gas, $E_{oxi}$ and $E_{cap}$ were increased by about 8%. This result was attributed to that in the presence of gas phase $O_2$, $SO_2$ could be oxidized by chemisorbed oxygen, which was generated due to $Ce^{3+}$ related charge imbalance, to form $SO_3$ [36]. And $SO_3$ could react with $Hg^0$ to produce $HgSO_4$ [29]. The two redox reactions are proposed as follows:

$$SO_2 + 1/2O_2 \rightarrow SO_3 \quad (13)$$

$$Hg^0 + 1/2O_2 + SO_3 \rightarrow HgSO_4 \quad (14)$$

*3.3.4. Effect of $H_2O$ (g)*

$H_2O$ (g) unavoidably exists in coal-combustion flue gas and has significant impact on the activities of the samples. So it was extremely important to evaluate the $H_2O$-resistance of the samples for possible industrial application in actual flue gas atmosphere. Fig. 8 shows that when 8% water vapor was added into the gas stream, $Hg^0$ removal efficiency declined by 15%. The inhibition of $H_2O$ could be attributed to competitive adsorption between water vapor and $Hg^0$ as report in previous studies [53]. Furthermore, the adsorbed $H_2O$ would react with $SO_3$ to form $H_2SO_4$ and the formed $H_2SO_4$ would further react with $CeO_2$ to form $Ce(SO_4)_2$. Both of the two compounds could cover the surface of sample and went against the $Hg^0$ removal. It should be noted that this series of experiments merely aimed to study the mechanisms; therefore, only 0.1 g sample was used. In comparison with set 1 and set 2 experiments, using more active samples with a larger amount may mitigate the adverse effect of $H_2O$. Additionally, the inhibitory effect of $H_2O$ could be outweighed by the promotional effects of $O_2$ and NO in the full gas.

## 4. Conclusions

In the present paper, the $Hg^0$ removal efficiencies of AICC were studied in a lab-scale fixed-bed system. Results showed that the $Hg^0$ oxidation and capture efficiency of AICC was higher than AC under the simulated flue gas condition. Especially, when the $CeCl_3$ loading was 6%, $Hg^0$ removal capability reached optimal value. In addition, temperature experiments showed that $Hg^0$ removal efficiency increased at first and then decreased with the rise of temperature from 110 to 230 °C, and the optimal temperature was about 170 °C. Moreover, NO in the flue gas was observed to promote $Hg^0$ oxidation, while $H_2O$ (g) inhibited $Hg^0$ oxidation. $SO_2$ promoted $Hg^0$ oxidation in the presence of $O_2$, while it showed an insignificant inhibition of $Hg^0$ oxidation without $O_2$ in the flue gas. The analysis results of XRD and XPS indicated that $Ce_xO_y$ and C–Cl were generated on the surface of AICC. During the adsorption and oxidation process, the $Hg^0$ could react with the active elements such as $CeO_2$ or C–Cl and was mainly in the form of mercuric oxide (HgO) and mercuric chloride ($HgCl_2$). The reactions for $Hg^0$ conversion indicated that activated coke loaded with cerium chloride possessed a catalytic effect of valence variable cerium and $Hg^0$ oxidation favored by chloride presence. Considering the necessity and possibility of the regenerability of the AICC sorbent-catalyst, a further investigation on this issue will be carried out.

## Acknowledgements

This work was supported by the National High Technology Research and Development Program of China (863 Program, No. 2011AA060803), the Scientific and Technological Major Special Project of Changsha City in China (No. K0902006-31), the Scientific and Technological Major Special Project of Hunan Province in China (No. 2010XK6003), the National Natural Science Foundation of China (No. 51108169), the Scientific and Technological Project of Hunan Province in China (No. 2011SK3219).

## References

[1] United Nations Environment Programme (UNEP), Global Mercury Assessment, UNEP Chemicals, Geneva, Switzerland, December, 2002.
[2] J.H. Pavlish, E.A. Sondreal, M.D. Mann, E.S. Olson, K.C. Galbreath, D.L. Laudal, S.A. Benson, Status review of mercury control options for coal-fired power plants, Fuel Process. Technol. 82 (2003) 89–165.

[3] A.A. Presto, E.J. Granite, Survey of catalysts for oxidation of mercury in flue gas, Environ. Sci. Technol. 40 (2006) 5601–5609.
[4] US EPA. Final Mercury and Air Toxics Standards (MATS) for Power Plants. Final Rule. <http://www.epa.gov/airquality/powerplanttoxics/actions.html> (effective on 19.04.12).
[5] State Environmental Protection Administration of China (SEPA), Emission Standard of Air Pollution for Thermal Power Plants, GB 13223-2011, SEPA, Beijing, 2011.
[6] K. Sundseth, J.M. Pacyna, E.G. Pacyna, J. Munthe, M. Belhaj, S. Astrom, Economic benefits from decreased mercury emissions: Projections for 2020, J. Cleaner Production 18 (2010) 386–394.
[7] B. Krishnakumar, J.J. Helble, Understanding mercury transformations in coal-fired power plants: evaluation of homogeneous Hg oxidation mechanisms, Environ. Sci. Technol. 41 (2007) 7870–7875.
[8] E.J. Granite, C.R. Myers, W.P. King, D.C. Stanko, H.W. Pennline, Sorbents for mercury capture from fuel gas with application to gasification systems, Ind. Eng. Chem. Res. 45 (2006) 4844–4848.
[9] N.Q. Yan, S.H. Liu, S.G. Chang, C. Miller, Method for the study of gaseous oxidants for the oxidation of mercury gas, Ind. Eng. Chem. Res. 44 (2005) 5567–5574.
[10] Y. Wang, Y. Liu, Z. Wu, J. Mo, B. Cheng, Experimental study on the absorption behaviors of gas phase bivalent mercury in Ca-based wet flue gas desulfurization slurry system, J. Hazard. Mater. 183 (2010) 902–907.
[11] Y. Cao, Z. Gao, J. Zhu, Q. Wang, Y. Huang, C. Chiu, B. Parker, P. Chu, W.-P. Pan, Impacts of halogen additions on mercury oxidation, in a slipstream selective catalyst reduction (SCR), reactor when burning sub-bituminous coal, Environ. Sci. Technol. 42 (2008) 256–261.
[12] S. Yang, N. Yan, Y. Guo, D. Wu, H. He, Z. Qu, J. Li, Q. Zhou, J. Jia, Gaseous elemental mercury capture from flue gas using magnetic nanosized $(Fe_{3-x}Mn_x)_{1-\delta}O_4$, Environ. Sci. Technol. 45 (2011) 1540–1546.
[13] W. Liu, R.D. Vidic, T.D. Brown, Impact of flue gas conditions on mercury uptake by sulfur-impregnated activated carbon, Environ. Sci. Technol. 34 (2000) 154–159.
[14] S.B. Ghorishi, R.M. Keeney, S.D. Serre, B.K. Gullett, W.S. Jozewicz, Development of a Cl-impregnated activated carbon for entrained-flow capture of elemental mercury, Environ. Sci. Technol. 36 (2002) 4454–4459.
[15] S.J. Lee, Y.-C. Seo, J. Jurng, T.G. Lee, Removal of gas-phase elemental mercury by iodine-and chlorine-impregnated activated carbons, Atmos. Environ. 38 (2004) 4887–4893.
[16] Z. Mei, Z. Shen, Q. Zhao, W. Wang, Y. Zhang, Removal and recovery of gas-phase mercury by metal oxide-loaded activated carbon, J. Hazard. Mater. 152 (2008) 721–729.
[17] G.A. Norton, H. Yang, R.C. Brown, D.L. Laudal, Heterogeneous oxidation of mercury in simulated post combustion conditions, Fuel 82 (2003) 107–116.
[18] K.C. Galbreath, C.J. Zygarlicke, E.S. Olson, J.H. Pavlish, D.L. Toman, Evaluating mercury transformation mechanisms in a laboratory-scale combustion system, Sci. Total Environ. 261 (2000) 149–155.
[19] C. Senior, C.J. Bustard, M. Durham, K. Baldrey, D. Michaud, Characterization of fly ash from full-scale demonstration of sorbent injection for mercury control on coal-fired power plants, Fuel Process. Technol. 85 (2004) 601–612.
[20] C.W. Lee, R.K. Srivastave, S.B. Ghorishi, T.W. Hastings, F.M. Stevens, Investigation of selective catalytic reduction impact on mercury speciation under simulated $NO_x$ emission control conditions, J. Air Waste Manage. Assoc. 54 (2004) 1560–1566.
[21] R. Mangal, B.R. Seckington, K. Zanganeh, R. Dureau, Effects of a mercury oxidant on SCR catalyst for PRB coal, in: International Conference on Air Quality IVs Mercury, Trace Elements, and Particulate Matter; Arlington, VA, 2003.
[22] A.P. Jones, J.W. Hoffmann, D.N. Smith, T.J. Feeley, J.T. Murphy, DOE/NETL' phase II mercury control technology field testing program: preliminary economic analysis of activated carbon injection, Environ. Sci. Technol. 41 (2007) 1365–1371.
[23] Z. Luo, C. Hu, J. Zhou, K. Cen, Stability of mercury on three activated carbon sorbents, Fuel Process. Technol. 87 (2006) 679–685.
[24] D.G. Olson, K. Tsuji, I. Shiraishi, The reduction of gas phase air toxics from combustion and incineration sources using the MET–Mitsui–BF activated coke process, Fuel Process. Technol. 65–66 (2000) 393–405.
[25] K. Tsuji, I. Shiraishi, Combined desulfurization, denitrification and reduction of air toxics using activated coke 1. Activity of activated coke, Fuel 76 (1997) 549–553.
[26] Z.Y. Feng, Technologies of preparation and application of activated coke, Dalian University of Technology Press, pp. 9–11, pp. 89–104, (in Chinese).
[27] K. Tsuji, I. Shiraishi, Combined desulfurization, denitrification and reduction of air toxics using activated coke 2. Process applications and performance of activated coke, Fuel 76 (1997) 555–560.
[28] L. Tian, C. Li, Q. Li, G. Zeng, Z. Gao, S. Li, X. Fan, Removal of elemental mercury by activated carbon impregnated with $CeO_2$, Fuel 88 (2009) 1687–1691.
[29] X. Fan, C. Li, G. Zeng, Z. Gao, L. Chen, W. Zhang, H. Gao, Removal of gas-phase element mercury by activated carbon fiber impregnated with $CeO_2$, Energy Fuels 24 (2010) 4250–4254.
[30] X. Wen, C. Li, X. Fan, H. Gao, W. Zhang, L. Chen, G. Zeng, Y. Zhao, Experimental study of gaseous elemental mercury removal with $CeO_2/\gamma$-$Al_2O_3$, Energy Fuel 25 (2011) 2939–2944.
[31] Q. Wan, L. Duan, K. He, J. Li, Removal of gaseous elemental mercury over a $CeO_2$–$WO_3/TiO_2$ nanocomposite in simulated coal-fired flue gas, Chem. Eng. J. 170 (2011) 512–517.
[32] J.-Y. Lee, Y. Ju, S.-S. Lee, T.C. Keener, R.S. Varma, Novel mercury oxidant and sorbent for mercury emissions control from coal-fired power plants, Water Air Soil Pollut.: Focus 8 (2008) 333–341.
[33] S.-S. Lee, J.-Y. Lee, T.C. Keener, Bench-scale studies of in-duct mercury capture using cupric chloride-impregnated carbons, Environ. Sci. Technol. 43 (2009) 2957–2962.
[34] C. Hu, J. zhou, S. He, Z. Luo, K. Cen, Effect of chemical activation of an activated carbon using zinc chloride on elemental mercury adsorption, Fuel Process. Technol. 90 (2009) 812–817.
[35] T.R. Carey, O.W. Hargrove Jr., C.F. Richardson, R. Chang, F.B. Meserole, Factors affecting mercury control in utility flue gas using activated carbon, J. Air Waste Manag. Assoc. 48 (12) (1998) 1166–1174.
[36] H. Li, C.-Y. Wu, Y. Li, J. Zhang, $CeO_2$–$TiO_2$ catalysts for catalytic oxidation of elemental mercury in low-rank coal combustion flue gas, Environ. Sci. Technol. 45 (2011) 7394–7400.
[37] Y. Ch Xie, Y.Q. Tang, Spontaneous monolayer dispersion of oxides and salts onto surfaces of supports: applications to heterogeneous catalysis, Adv. Catal. 37 (17) (1990) 1–43.
[38] N.D. Hutson, B.C. Attwood, K.G. Scheckel, XAS and XPS characterization of mercury binding on brominated activated carbon, Environ. Sci. Technol. 41 (2007) 1747–1752.
[39] X. Hua, J. Zhou, Q. Li, Z. Luo, K. Cen, Gas-phase elemental mercury removal by $CeO_2$ impregnated activated coke, Energy Fuels 24 (2010) 5426–5431.
[40] G.E. Muilenberg, (Ed.), The Handbook of X-ray Photoelectron Spectroscopy, Perkin-Elmer Corp., 1979.
[41] A.F. Perez-Cadenas, F.J. Maldonado-Hodar, C. Moreno-Castilla, On the nature of surface acid sites of chlorinated activated carbons, Carbon 41 (2003) 473–478.
[42] X.J. Zhou, K.T. Leung, Modification of electronic structure of mesoscopic perchlorate-doped polypyrrole films by ion irradiation, Macromolecules 36 (2003) 2882–2885.
[43] B.M. Reddy, A. Khan, Y. Yamada, T. Kobayashi, S. Loridant, J.-C. Volta, Structural characterization of $CeO_2$–$TiO_2$ and $V_2O_5/CeO_2$–$TiO_2$ catalysts by Raman and XPS techniques, J. Phys. Chem. B 107 (2003) 5162–5167.
[44] X. Gao, Y. Jiang, Y. Zhong, Z. Luo, K. Cen, The activity and characterization of $CeO_2$–$TiO_2$ catalysts prepared by the sol–gel method for selective catalytic reduction of NO with $NH_3$, J. Hazard. Mater. 174 (2010) 734–739.
[45] Z. Shen, J. Ma, Z. Mei, J. Zhang, Metal chlorides loaded on activated carbon to capture elemental mercury, J. Environ. Sci. 22 (2010) 1814–1819.
[46] Y. Li, P.D. Murphy, C.-Y. Wu, K.W. Powers, J.-C.J. Bonzongo, Development of silica/vanadia/titania catalysts for removal of elemental mercury from coal-combustion flue gas, Environ. Sci. Technol. 42 (2008) 5304–5309.
[47] H. Li, Y. Li, C.-Y. Wu, J. Zhang, Oxidation and capture of elemental mercury over $SiO_2$–$TiO_2$–$V_2O_5$ catalysts in simulated low-rank coal combustion flue gas, Chem. Eng. J. 169 (2011) 186–193.
[48] R.D. Vidic, D.P. Siler, Vapor-phase element mercury adsorption by activated carbon impregnated with chloride and chelating agents, Carbon 39 (2001) 3–14.
[49] M.H. Kim, S.-W. Ham, J.-B. Lee, Oxidation of gaseous elemental mercury by hydrochloric acid over $CuCl_2/TiO_2$-based catalysts in SCR process, Appl. Catal. B 99 (2010) 272–278.
[50] S.J. Miller, G.E. Dunham, E.S. Olson, T.D. Brown, Flue gas effects on a carbon-based mercury sorbent, Fuel Process. Technol. 65–66 (2000) 343–363.
[51] J. Liu, W. Qu, S.W. Joo, C. Zheng, Effect of $SO_2$ on mercury binding on carbonaceous surfaces, Chem. Eng. J. 184 (2012) 163–167.
[52] D.L. Laudal, T.D. Brown, B.R. Nott, Effects of flue gas constituents on mercury speciation, Fuel Process. Technol. 65–66 (2000) 157–165.
[53] Y. Li, C.-Y. Wu, Role of moisture in adsorption, photocatalytic oxidation, and reemission of elemental mercury on a $SiO_2$–$TiO_2$ nanocomposite, Environ. Sci. Technol. 40 (2006) 6444–6448.